Asymmetric comb waveguide for strong interactions between atoms and light

N Fayard, A Bouscal, J Berroir, A Urvoy, T Ray, S Mahapatra, M Kemiche, Juan Ariel Levenson, Jean-Jacques Greffet, K. Bencheikh, et al.

Asymmetric comb waveguide for strong interactions between atoms and light

N. Fayard,[1] A. Bouscal,[2] J. Berroir,[2] A. Urvoy,[2] T. Ray,[2] S. Mahapatra,[3] M. Kemiche,[3,4] J. A. Levenson,[3] J.-J. Greffet,[1] K. Bencheikh,[3] J. Laurat,[2] and C. Sauvan[1,*]

[1]*Université Paris-Saclay, Institut d'Optique Graduate School, CNRS, Laboratoire Charles Fabry, 91127 Palaiseau, France*
[2]*Laboratoire Kastler Brossel, Sorbonne Université, CNRS, ENS-Université PSL, Collège de France, 4 place Jussieu, 75005 Paris, France*
[3]*Université Paris-Saclay, CNRS, Centre de Nanosciences et de Nanotechnologies, 91120 Palaiseau, France*
[4]*Currently with Université Grenoble Alpes, Université Savoie Mont Blanc, CNRS, Grenoble INP, IMEP-LAHC, 38000 Grenoble, France*
[*]*christophe.sauvan@institutoptique.fr*

Abstract: Coupling quantum emitters and nanostructures, in particular cold atoms and optical waveguides, has recently raised a large interest due to unprecedented possibilities of engineering light-matter interactions. In this work, we propose a new type of periodic dielectric waveguide that provides strong interactions between atoms and guided photons with an unusual dispersion. We design an asymmetric comb waveguide that supports a slow mode with a quartic (instead of quadratic) dispersion and an electric field that extends far into the air cladding for an optimal interaction with atoms. We compute the optical trapping potential formed with two guided modes at frequencies detuned from the atomic transition. We show that cold Rubidium atoms can be trapped as close as 100 nm from the structure in a 1.3-mK-deep potential well. For atoms trapped at this position, the emission into guided photons is largely favored, with a beta factor as high as 0.88 and a radiative decay rate into the slow mode 10 times larger than the free-space decay rate. These figures of merit are obtained at a moderately low group velocity of $c/50$.

1. Introduction

The development of quantum technologies requires a number of prerequisites among which strong atom-photon interactions hold a high rank [1, 2]. Enhancing the interaction between a single photon and a single atom has been a driving force for a large community over the past decades. Two main routes have been followed rather independently: atoms in macroscopic high-finesse cavities [3, 4] or solid-state emitters (e.g., quantum dots) in micro and nanostructures [5, 6]. In recent years, various works have combined both approaches by interfacing cold atoms with nanophotonic devices such as photonic crystal nanocavities [7], nanofibers [8–10], and photonic crystal waveguides [11–13]. These hybrid strategies benefit from both the long coherence time of atoms and the enhanced electromagnetic field associated with subwavelength light confinement.

Besides the well-established field of cavity quantum electrodynamics (QED), the use of single-pass schemes with nanofibers or nanostructured waveguides has triggered the emergence of a new field of research known as waveguide QED [14–16]. Photons travelling in the waveguide carry the information through long distances while atoms can store it for long times. These systems are a promising building block for quantum networks as shown recently by the experimental demonstrations of a coherent photon storage [17, 18], the heralded creation of a single collective excitation of atomic arrays [19], or a correlated photon transport [20–22]. In addition, strong atom-photon interactions give rise to new phenomena in many-body physics [23] such as the emergence of solitons dynamics [24, 25] or many-body localization [26].

Most of the existing experiments in waveguide QED at optical frequencies are performed with silica nanofibers [8–10, 17–19, 22, 27–29]. They offer a 4π solid-angle access to the interaction region that markedly eases the manipulation of atomic clouds near the structure. In addition, nanofibers provide single-mode operation over a broad spectral range. It is thus possible to use guided light beams at frequencies detuned from the atomic transition for trapping the atoms at subwavelength distances from the waveguide [10, 30, 31]. However, the atom-photon interaction remains relatively weak. It can be quantified by the β factor, which is defined as the ratio of the radiative decay rate of a single atom in the waveguide mode Γ_{1D} to the total decay rate Γ_{tot}, $\beta = \Gamma_{1D}/\Gamma_{tot} = \Gamma_{1D}/(\Gamma_{1D} + \Gamma')$. Photons that are not funnelled into the waveguide mode are lost in the radiation continuum with a decay rate Γ'. Experimentally observed values of β in nanofibers are typically in the range of $\beta \sim 0.05$ [32–34].

A promising route to increase Γ_{1D} and β is to use periodic dielectric waveguides, i.e., waveguides with a periodic modulation of the refractive index along the propagation direction. Indeed, the radiative decay rate of a single atom in a guided mode is given by $\Gamma_{1D}/\Gamma_0 = n_g\sigma/(2A_{\text{eff}})$, where Γ_0 is the atomic decay rate in free space, σ is the absorption cross-section, n_g and A_{eff} are the group index of the mode and the effective area at the atom position [11, 35]. In periodic waveguides, the coupling between contrapropagating modes results in the opening of bandgaps in the dispersion relation and in the apparition of band edges where the group velocity $v_g = c/n_g$ goes to zero [36]. Close to these peculiar points, periodic waveguides support slow guided modes with large n_g's, which, in turn, lead to increased values of Γ_{1D} and β [35]. Hence, an important research effort has been devoted to the design and the realization of periodic waveguides aimed at increasing the interaction with cold atoms [11–13, 37, 38]. However, this is a challenging task that requires tackling various issues [13, 39], including the sensitivity of slow light to fabrication imperfections, a stable trapping of atoms at the desired positions, and the accessibility around the structure to ease the transport of the atoms to the trapping sites.

In addition to enhanced atom-photon interactions, periodic waveguides also offer the possibility to create dispersion relations that greatly differ from the usual and almost linear dispersion of a nanofiber. The curvature of the dispersion relation between the frequency ω and the wavevector k has a profound impact on various physical phenomena, such as the distortion of short pulses during propagation, the collective properties of atomic arrays coupled to the waveguide, the localization of photons emitted in the bandgap [15], as well as the tolerance of the slow mode to inevitable fabrication imperfections [13, 40]. However, the engineering of the dispersion has been quite limited until now. Indeed, most of the periodic waveguides studied so far (be it for interacting with atoms or for another purpose) are made of a periodic pattern that is symmetric in transverse directions [11, 12, 36, 37, 41–47] and their dispersion relation varies most often quadratically at band edges.

By breaking the transverse symmetry, one can obtain new degrees of freedom for engineering the dispersion beyond the standard parabolic shape. Recently, Nguyen *et al.* demonstrated with a two-dimensional (2D) structure that symmetry breaking can be used to create exotic photonic dispersion relations such as Dirac cones, multivalley curves, or flat bands [48].

In this article, we exploit symmetry breaking to design a novel three-dimensional (3D) geometry, the asymmetric comb waveguide, that (i) supports a slow mode with a *quartic* dispersion, (ii) offers the possibility to trap atoms optically at subwavelength distances, and (iii) provides very large β factors for trapped atoms. We show that the quartic dispersion makes the slow mode more tolerant to fabrication imperfections than previous proposals [13]. The structure is represented in Fig. 1. It consists of a suspended bridge waveguide of width H and thickness t_y that has been periodically corrugated with an asymmetric rectangular pattern. This structure opens new opportunities in waveguide QED since it provides both a strong atom-photon interaction and an unusual dispersion that differs from the standard parabolic shape.

The article is organized as follows. In Section 2, we illustrate with 2D examples the role of

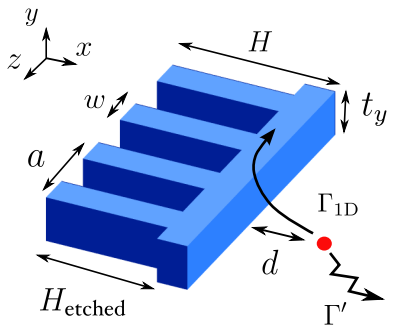

Fig. 1. Scheme of the asymmetric comb waveguide. The structure is etched in a GaInP membrane (refractive index $n = 3.31$) suspended in air. The waveguide has a total width H in the transverse x direction and a thickness t_y in the transverse y direction. The comb pattern along the propagation direction z is made of teeth with a width w and a height H_{etched}, periodically spaced with a period a. The width of the guiding region is thus $H - H_{\text{etched}}$. An excited atom (red dot) decays radiatively either into the guided mode, with a rate Γ_{1D}, or into the radiation continuum with a rate Γ'.

symmetry breaking in the design of a flat band with a quartic dispersion. Then, we design in Section 3 a 3D comb waveguide with a quartic dispersion after having detailed a few important criteria that should be fulfilled by a periodic waveguide aimed at interacting with cold atoms. We present in Section 4 the calculation of the potential of a two-color optical trap made with guided modes. We show that cold Rubidium (Rb) atoms can be trapped as close as 100 nm from the waveguide in a 1.3-mK-deep potential well by using relatively low powers ($P \sim 1$ mW) compatible with photonic structures. Finally, we calculate in Section 5 the emission rates Γ_{1D}, Γ_{tot}, and Γ' of a trapped atom. We provide evidence for very large coupling between the atom and a slow mode with $n_g = 50$: $\Gamma_{1D} = 10\Gamma_0$, $\Gamma' = 1.3\Gamma_0$, and $\beta = 0.88$. Section 6 concludes the work and discusses some perspectives.

2. Slow mode with a quartic dispersion

In this Section, we show that symmetry breaking can be used to create a comb waveguide that supports a slow mode with a quartic dispersion around a zero-group-velocity point instead of the usual parabolic shape. In order to illustrate the impact of symmetry breaking, we compare the band diagrams of four different periodic waveguides with a period a. The waveguides are schematically represented in the insets of Figs. 2(a)-(d). All four are comb waveguides (see Fig. 1) with the same total width $H = 2a$ but different corrugations. The comparison is done with 2D structures ($t_y = \infty$) in TM polarization (magnetic field polarized in the y direction). We consider a refractive index $n = 2.85$ that corresponds to the effective index of the fundamental guided mode in a GaInP membrane of thickness 150 nm at $\lambda = 780$ nm.

The dispersion curves are calculated with a Bloch-mode solver developed for studying light scattering in periodic waveguides [49]. The solver calculates the wavevector k in the propagation direction as a function of the frequency ω. It is implemented with the aperiodic Fourier modal method (a-FMM) [50], which relies on an analytical integration of Maxwell's equations along the direction of periodicity (z axis) and on a supercell approach with perfectly-matched layers (PMLs) along the transverse directions (x and y axis). PMLs ensure a correct treatment of far-field radiation conditions; they are implemented as complex nonlinear coordinate transforms [51]. This numerical method is also used in the rest of the paper for the calculation of the field distributions and the decay rates.

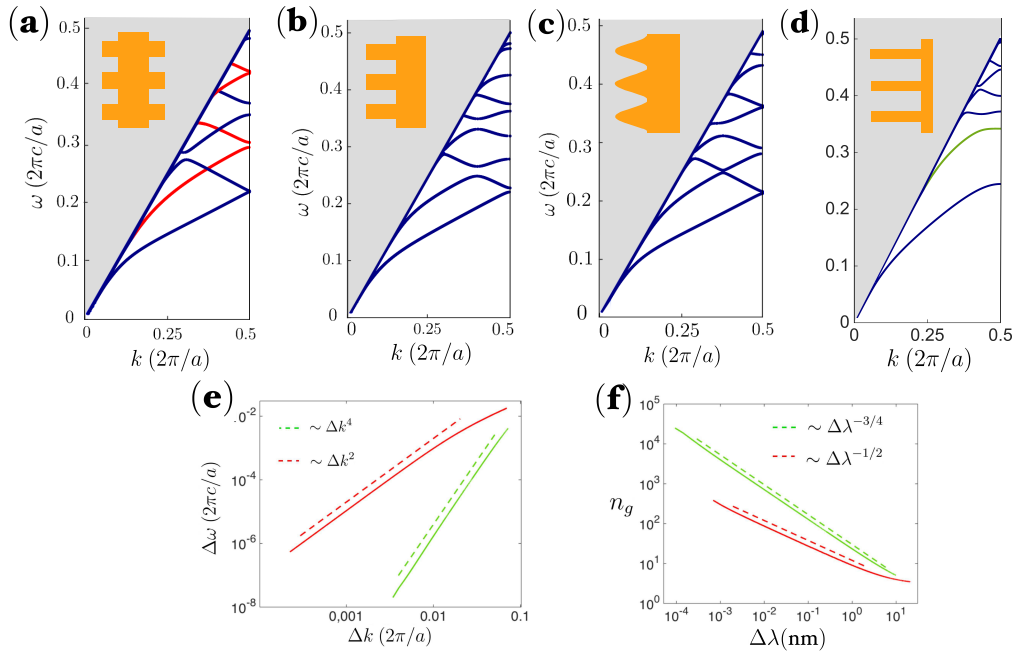

Fig. 2. Impact of a transverse symmetry breaking. (a)-(d) Band diagram $\omega = f(k)$ of four different 2D comb waveguides in TM polarization. The height of all structures is $H = 2a$, with a the period. To bring these 2D calculations closer to 3D simulations, we consider an effective refractive index $n = 2.85$. (a) Symmetric comb waveguide. The width of the teeth on both sides is $w = 0.5a$ and their depth is $H_{\text{etched}} = 0.25H$. (b) Asymmetric comb waveguide. The teeth are two times deeper, $H_{\text{etched}} = 0.5H$, with the same width $w = 0.5a$ to conserve the fraction of matter. (c) Asymmetric comb waveguide with a sinusoidal corrugation but the same fraction of matter. The depth of the cosine modulation is chosen so that the quantity of matter is the same as in (a)-(b). (d) Asymmetric comb waveguide designed to support a flat band with a quartic dispersion (green curve). The parameters are $w = 0.372a$ and $H_{\text{etched}} = 0.8H$. (e) Variation of $\Delta\omega = |\omega - \omega_e|$ as a function of $\Delta k = |k - \pi/a|$ in logarithmic scales (solid lines) for the green band in (d) and the red band of lowest frequency in (a). Dashed straight lines represent pure quadratic (slope of two in red) and quartic (slope of four in green) variations for comparison. (f) Group index as a function of $\Delta\lambda = |\lambda - \lambda_e|$. The quadratic and quartic dispersions lead to different scaling laws, as shown by the dashed straight lines that represent slopes of $-1/2$ (red) and $-3/4$ (green).

Figure 2(a) displays the band diagram of a comb waveguide whose corrugation is symmetric in the transverse direction. It can be easily understood with the following picture: the uncorrugated planar waveguide of width H supports symmetric and antisymmetric modes and the periodic corrugation couples forward and backward propagating modes, resulting in the opening of photonic bandgaps [36]. However, the symmetry of the corrugation forbids coupling between modes of different symmetry. Therefore, the Bloch modes resulting from the coupling can be sorted in two distinct families: they are either symmetric (blue curves) or antisymmetric (red curves). As can be seen, blue and red curves cross each other without coupling. Most of the bandgaps and the associated zero-group-velocity points are located at the edge of the first Brillouin zone, at $k = \pi/a$. Using a standard coupled-mode approach with two waves having linear dispersions, one can show that the dispersion relation of the Bloch modes varies quadratically in the vicinity of these points: $\omega - \omega_e \propto \pm(k - \pi/a)^2$, where ω_e is the frequency

of the band edge where $v_g = 0$ (see Supplement 1 for more details).

We now consider in Figs. 2(b)-(c) comb waveguides without mirror symmetry in the transverse direction and with two different corrugations profiles. For the sake of comparison, the fraction of matter (the orange area) is the same as in Fig. 2(a). The situation is now fundamentally different: since the corrugations have no particular symmetry, all possible couplings are indeed allowed. As a result, gaps are now open inside the Brillouin zone ($k \neq \pi/a$) around the points of intersection between the dispersion curves of the symmetric and antisymmetric modes of the uncorrugated waveguide. Looking precisely to the band diagrams, we observe that the spectral widths of the bandgaps are smaller for a sinusoidal profile than for a rectangular profile. Thus, the latter provides larger coupling strengths. This is the reason why we study the rectangular asymmetric comb waveguide in the following.

For a rectangular profile, the coupling strengths depend on the size of the teeth, fixed by the width w and the depth H_{etched} defined in Fig. 1. Stronger corrugations result in larger coupling strengths and wider bandgaps. If the coupling is strong enough, two consecutive bandgaps may overlap. In this case, the coupling mechanism is more complex since it involves four waves instead of two [48]. This offers extra degrees of freedom for engineering the bands beyond the standard parabolic shape.

Following this principle, we have designed an asymmetric comb waveguide that supports a flat band with a *quartic* dispersion curve of the form $\omega - \omega_e \propto -(k - \pi/a)^4$. This flat band is highlighted in green in Fig. 2(d). In order to confirm the quartic variation, we plot in Fig. 2(e) $\Delta\omega = |\omega - \omega_e|$ as a function of $\Delta k = |k - \pi/a|$ with logarithmic scales. The solid green curve is extracted from the green band in Fig. 2(d). It follows a quartic variation, parallel to the dashed green straight line with a slope of four. In contrast, the symmetric comb waveguide of Fig. 2(a) (solid red curve) supports modes with a quadratic dispersion, as shown by the dashed red straight line that represents a slope of two.

A flat band with a quartic dispersion broadens the useful bandwidth of the slow mode, i.e., the bandwidth over which n_g is larger than a target value. Indeed, a quartic dispersion produces a group index that scales with the wavelength as $\Delta\lambda^{-3/4}$ while the group index of a quadratic dispersion scales as $\Delta\lambda^{-1/2}$. These scaling laws are derived in Supplement 1 and probed in Fig. 2(f). Therefore, if one wants to work at a given group index, the quartic dispersion (green curve) allows an operation at a larger $\Delta\lambda$, i.e., at a frequency further from the band edge. We will see in the next Section that this increase of the useful bandwidth is important to improve the tolerance of the slow mode to fabrication imperfections.

Let us end this Section by emphasizing that a quartic functional form for the dispersion relation of a slow mode is uncommon, in particular in the context of waveguide QED where it has not been studied so far. It is thus important to design a waveguide with a quartic dispersion and a 3D geometry compatible with the interaction with cold atoms trapped in the air cladding. We present this design in the following Section.

3. Design of a three-dimensional asymmetric comb waveguide

We first detail a few important requirements that apply to a slow-light waveguide designed to interact with cold atoms. Then, we present the design of a 3D asymmetric comb waveguide that supports a slow mode with a quartic dispersion at the transition frequency of Rb atoms and an evanescent field that extends far into the air cladding for an optimal interaction. In addition, we pay particular attention during the design process to the presence of blue- and red-detuned modes that can be used to create an optical two-color trap.

3.1. Design requirements

The design of a periodic waveguide aimed at increasing the coupling with cold atoms should maximize the emission rate into the waveguide mode Γ_{1D}. Since the group index diverges at a

band edge, the first idea is to align the transition frequency of the atom with any band edge of the photonic dispersion diagram. Unfortunately, this simple design cannot work for several reasons.

First, slow light is very sensitive to fabrication imperfections, resulting in backscattering, radiation losses, and potentially light localization [40, 52–54]. Therefore, in a practical situation, fabrication imperfections set an upper bound to the group index n_g that can be reached [55–57]. To improve the fabrication tolerance, X. Zhang *et al.* proposed to use parabolic dispersion curves with large effective photon masses, $m_{\text{eff}} = \left(\partial^2\omega/\partial k^2\right)^{-1}$ [13]. Therefore, the design should not only increase the group index, but also reduce the curvature of the dispersion relation.

A second issue is the value of the effective mode area at the position of the atom, or equivalently the effective cross section of the photon seen by the atom. One should be careful not to lose with an increased mode area what is gained with an increased group index. Hence, the design has to find a trade-off between two opposite trends. On the one hand, we need a mode whose field extends far into the air cladding, implying that it weakly interacts with the periodic pattern. On the other hand, we need to control the group velocity and the curvature of the dispersion relation, meaning that we need a mode that strongly interacts with the periodic pattern.

Finally, a third important challenge is to generate a stable optical trap for the atoms at subwavelength distances of the waveguide and to be able to bring the atoms inside the trap. A fully integrated trapping scheme can be achieved by using "fast" guided modes (i.e., with standard values of n_g) at frequencies detuned from the atomic transition. For instance, red- and blue-detuned modes can be used to create a two-color trap [31]. The design of the periodic waveguide should thus ensure the presence of additional modes with adequate field profiles, which spatially overlap with each other and with the slow mode.

As a whole, the design of a periodic waveguide with increased atom-photon interactions is a complex task that should meet the following criteria:

1. a slow and single-mode operation at the transition frequency of the atom (large n_g),
2. a large fraction of the electric field in air outside the structure (small A_{eff}),
3. a large effective photon mass for an improved robustness to fabrication imperfections,
4. the existence of additional modes at frequencies detuned from the atomic transition for trapping the atoms optically with low powers (few mW),
5. a clear access around the structure to ease the transport of the atoms to the trapping sites.

Up to now, two main geometries have been investigated. The first one, the alligator waveguide, is composed of a tiny 250-nm-wide air slot symmetrically surrounded by two corrugated bridge waveguides [11, 12, 38]. This geometry fulfills the first two criteria (large n_g and small A_{eff}) as well as the fourth one. However, it has been shown in [13] that the effective photon mass of the slow mode is small, meaning that alligator waveguides are very sensitive to fabrication imperfections in the slow-light regime. The fifth criterion is not met either since the atoms need to be loaded in a narrow interacting region, which constitutes a major experimental challenge [58]. External trapping via side illumination has been considered [39, 59], but a stable trapping of atoms *inside* the air slot has not been demonstrated. As a result, the value of β and the number N of trapped atoms are limited to $\beta \sim 0.5$ and $N \sim 3$ [12, 60].

A different geometry has been proposed in [13] to address these limitations. It consists of a hybrid-clad waveguide that combines two guidance mechanisms: total internal reflection on one lateral side with a sharp sidewall and photonic bandgap on the opposite lateral side with a two-dimensional photonic crystal. The hybrid-clad waveguide provides a flatter dispersion curve than the alligator waveguide (50 times enhanced effective photon mass) and a 2π solid-angle access to the interaction region. However, the possibility to use detuned guided beams for trapping the atoms (fourth criterion) has not been investigated yet. One the one hand, the bandgap of the photonic-crystal cladding sets important constraints on the spectral range available to place

additional guided modes that could be used for trapping. On the other hand, the photonic-crystal geometry provides various degrees of freedom for engineering the band diagram.

In the following, we design an asymmetric comb waveguide that fulfills all five criteria. In addition, the dispersion relation of the slow mode is quartic instead of quadratic. We show that, thanks to the quartic dispersion, the slow mode of the comb waveguide is more tolerant to fabrication imperfections than the mode of the hybrid-clad waveguide proposed in [13] that mostly follows a standard parabolic dispersion. To further limit the loss issues related to fabrication imperfections, we have chosen to use a moderately slow mode with $n_g = 50$, a value compatible with current fabrication processes [57]. We calculate in Section 5 that, despite this moderate slowdown of the light, we can achieve a strong atom/photon interaction.

3.2. Asymmetric comb waveguide

In order to benefit for a large refractive index contrast, we consider a GaInP membrane (refractive index $n = 3.31$) with a thickness $t_y = 150$ nm, as shown in Fig. 1. Starting from the 2D structure in Fig. 2(d), we have designed a 3D comb waveguide that supports a slow mode with a quartic dispersion $\omega - \omega_e \propto -(k - \pi/a)^4$ and a group index $n_g = 50$ at $\lambda_0 = 780$ nm, the wavelength of the $5S_{1/2} \leftrightarrow 5P_{3/2}$ transition of Rb atoms. The geometrical parameters are $a = 283$ nm, $H = 2a$, $H_{\text{etched}} = 0.8H$, and $w = 0.422a$. The band diagram of this comb waveguide is shown in Fig. 3(a); the slow mode with a quartic dispersion is highlighted in green. We consider the modes whose field components E_x, E_z, and H_y are symmetric with respect to $y = 0$.

Figures 3(b) and 3(c) display the distribution in the (x, z) plane of the dominant components of the electric field (E_x and E_z) at $\lambda_0 = 780$ nm. Note that the evanescent tail of the electric field extends far in the air cladding. On the side opposite the teeth, the longitudinal electric-field component E_z is maximum in front of the teeth, at $z \equiv a/2 \pmod a$. The positions of the maxima of the transverse electric-field component E_x are shifted by $a/2$, at $z \equiv 0 \pmod a$.

In addition to the slow mode, the band diagram should also provide two additional modes, red- and blue-detuned with respect to the atomic transition, that can be used to realize an optical two-color trap. These modes should lie below the light line and below the frequency of the electronic bandgap of GaInP ($\lambda = 680$ nm). The design of the structure has been performed by taking into account these additional constraints. The red- and blue-detuned modes are highlighted by the red and light blue dots in Fig. 3(a). The calculation of the trapping potential is presented in Section 4.

To ease the future implementation of the structure, it is important to keep in mind that nanostructured devices are never manufactured to their nominal specifications. Hence, real periodic waveguides are not exactly periodic and suffer from random fabrication imperfections. Slow light is particularly sensitive to these imperfections. It experiences random scattering as it propagates, resulting in backscattering, radiation losses, and possibly light localization [52–54].

In the usual case of a parabolic dispersion, the effective photon mass $m_{\text{eff}} = \left(\partial^2\omega/\partial k^2\right)^{-1}$ is the good figure of merit to be considered. It has been shown that a larger effective photon mass improves the tolerance of a slow mode to fabrication imperfections [13, 40]. According to these works, in the case of a non-parabolic dispersion, one must consider a second figure of merit in addition to the effective photon mass m_{eff}: the distance of the operation frequency to the band edge, $\Delta\omega = |\omega - \omega_e|$. To improve the tolerance to fabrication imperfections, both figures of merit should be increased: the effective photon mass *at the operation frequency* and the distance of the operation frequency to the band edge.

We have calculated m_{eff} and $\Delta\omega$ for the asymmetric comb. They are shown by the green curves in Figs. 3(d) and 3(e). For the sake of comparison, we have also calculated these figures of merit for the hybrid-clad waveguide proposed in [13], which is the most resilient to fabrication imperfections in the waveguide QED literature. Figure 3(d) displays the distance of the operation wavelength to the band edge, $\Delta\lambda = |\lambda - \lambda_e|$, as a function of the group index. Regardless of the

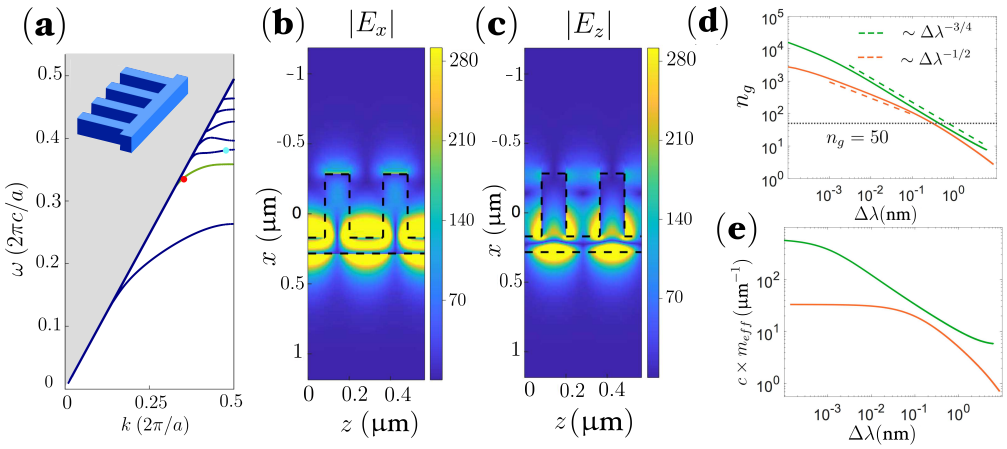

Fig. 3. Slow mode with a quartic dispersion. (a) Band diagram of the 3D comb waveguide designed to support a slow mode with a quartic dispersion (green curve) that stronly interacts with Rubidium atoms. The geometrical parameters are $a = 283$ nm, $H = 2a$, $H_{\text{etched}} = 0.8H$, $w = 0.422a$, $t_y = 150$ nm and $n = 3.31$. The red and light blue dots mark the "fast" modes red- ($\lambda_r = 837$ nm) and blue-detuned ($\lambda_b = 736$ nm) with respect to the atomic transition that are used for trapping, as detailed in Section 4. (b) Amplitude of the x-component of the slow mode electric field in V/µm. (c) Amplitude of the z-component of the slow mode electric field in V/µm. The field distributions are calculated for $\lambda_0 = 780$ nm at $y = 0$ in the middle of the membrane. (d) Group index as a function of the distance to the band edge, $\Delta\lambda = |\lambda - \lambda_e|$ (logarithmic scales). (e) Effective photon mass as a function of $\Delta\lambda = |\lambda - \lambda_e|$ (logarithmic scales). The green curves correspond to the slow mode of the 3D comb waveguide [green curve in (a)] and the orange curves correspond to the hybrid-clad waveguide in [13]. In (d), the dashed curves indicate the $\Delta\lambda^{-3/4}$ (green) and $\Delta\lambda^{-1/2}$ (orange) scaling laws.

value of the group index, the comb waveguide allows one to operate further from the band edge than the hybrid-clad waveguide. The dashed green and orange lines show that the asymmetric comb waveguide follows the scaling law that is expected for a quartic dispersion while the hybrid-clad waveguide mostly follows the scaling law of a quadratic dispersion. The dashed horizontal line marks the value $n_g = 50$ that is used in the following. Figure 3(e) shows the effective photon mass as a function of $\Delta\lambda$. Regardless of the operation frequency, the asymmetric comb has a larger effective mass than the hybrid-clad waveguide. Therefore, according to previous theoretical results [13, 40], the asymmetric comb waveguide should be more tolerant to fabrication imperfections than the hybrid-clad waveguide.

4. Two-color optical trap for Rubidium atoms

We show hereafter that the versatility of the asymmetric comb allows us to trap Rb atoms optically as close as 100 nm from the waveguide. At these deeply subwavelength distances, the atoms can strongly interact with the slow mode aligned with their transition frequency. The objective is to trap atoms where the electric field of the slow mode is intense, see Figs. 3(b)-(c). For accessibility reasons, it is not appropriate to create a trap between the comb teeth. Therefore, we aim at trapping atoms on the side opposite the teeth, see the red dot in Fig. 1.

There exist various ways to trap atoms close to a dielectric structure [30]. In waveguide QED, a smart, fully integrated, approach consists in taking advantage of the waveguide to build an optical trap with guided light beams. In this work, we use a two-color trap, whose principle is to send two additional light beams into the waveguide [31]. The first one is red detuned with respect

to the atomic transition; it produces a negative Stark shift on the energy of the ground state $5S_{1/2}$ that results in an attracting potential $U_r(x, y, z) < 0$. The second beam is blue detuned; it creates a positive Stark shift and a repulsive potential $U_b(x, y, z) > 0$. The combination of the two potentials,

$$U_{\text{trap}}(x, y, z) = U_r(x, y, z) + U_b(x, y, z), \tag{1}$$

can produce a deep potential well (i.e., a stable trap) at a given position in space that depends on the spatial profile of both guided beams, on their powers, and on the polarizability of the atom.

On top of the trapping potential U_{trap} generated by the detuned beams, it is necessary to take into account the attracting Casimir Polder (CP) potential that arises when an atom interacts with electromagnetic vacuum fluctuations near a dielectric surface [61, 62]. We assume that the CP potential felt by an atom close to the vertical sidewall of the comb (see the red dot in Fig. 1) is the same as the potential near a planar surface, which varies as $U_{\text{CP}} = -\frac{C_3}{d^3}$, where d is the distance between the atom and the surface and C_3 is a constant that depends both on the material and the atom. The value of C_3 for GaInP and Rb atoms, $C_3 \simeq 6.7 \times 10^4$ mK.nm^3, is computed with the formula in [63]; the permittivity of GaInP is taken from the experimental data in [64]. The desired depth of the trapping potential for cold atoms is typically of the order of 1 mK. In comparison, the CP potential is negligible for distances larger than 100 nm, $U_{\text{CP}}(100\text{ nm}) \approx -6.7 \times 10^{-2}$ mK, and it is dominant close to the surface $U_{\text{CP}}(10\text{ nm}) \approx -67$ mK.

In order to realize a two-color trap with guided modes, the frequencies of the detuned signals have to be chosen with the band diagram in Fig. 3(a). Since the waveguide is periodic, we are dealing with Bloch modes whose field distributions are periodically modulated along the z direction. It is thus possible to create a periodic array of potential wells in the z direction without using contra-propagating beams. It is convenient to choose the red-detuned frequency on the same band as the slow mode (green band), but closer to the light line where the group velocity is of the order of c/n. Then, one of the higher-order bands can be used for the blue-detuned frequency.

Since the wavelength of the $5S_{1/2} \leftrightarrow 5P_{3/2}$ transition of Rb atoms is $\lambda_0 = 780$ nm, we have chosen to work with $\lambda_r = 837$ nm for the red-detuned field and $\lambda_b = 736$ nm for the blue-detuned

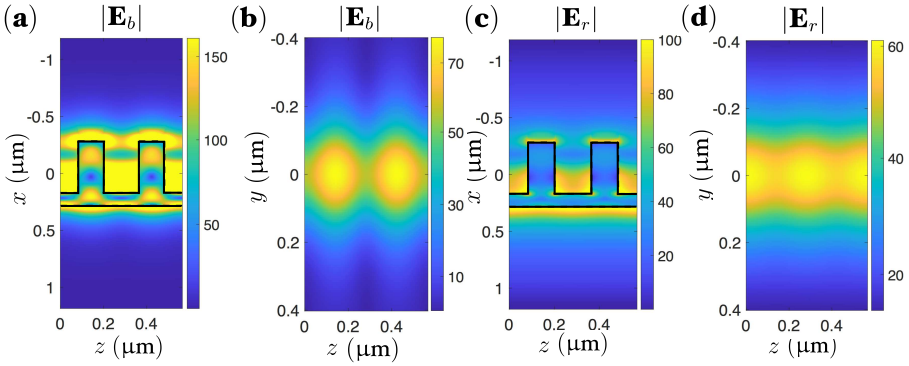

Fig. 4. Electric-field distributions of the blue- and the red-detuned guided modes used for the two-color trap. (a)-(b) Blue-detuned mode $\mathbf{E}_b$ at $\lambda_b = 736$ nm, marked by a light blue dot in the band diagram of Fig. 3(a). (c)-(d) Red-detuned mode $\mathbf{E}_r$ at $\lambda_r = 837$ nm, marked by a red dot in the band diagram of Fig. 3(a). In (a) and (c) the field is represented in the (x, z) plane at $y = 0$ (cross-section through the center of the GaInP membrane). The solid lines show the contour of the comb waveguide. In (b) and (d) the field is represented in a (y, z) plane located in air at a distance $d = 100$ nm from the structure. The fields are expressed in V/μm.

field. These wavelengths are displayed in Fig. 3(a) with red and light blue dots. The electric fields of the corresponding guided modes are shown in Fig. 4. The amplitude of the red-detuned mode is almost homogeneous in air along the z direction while the amplitude of the blue-detuned mode exhibits a more pronounced periodic modulation, with intensity maxima in front of the comb teeth at $z \equiv a/2 \pmod{a}$. Therefore, an atom near the back of the comb will "feel" an attracting potential that is almost independent of z and a repulsive potential that is stronger in front of the teeth. By playing with the relative powers of both detuned beams, it is possible to create a potential well with a minimum at $z \equiv 0 \pmod{a}$. An atom trapped at this position will interact efficiently with the slow mode since the transverse component of its electric field is maximum, see Fig. 3(b).

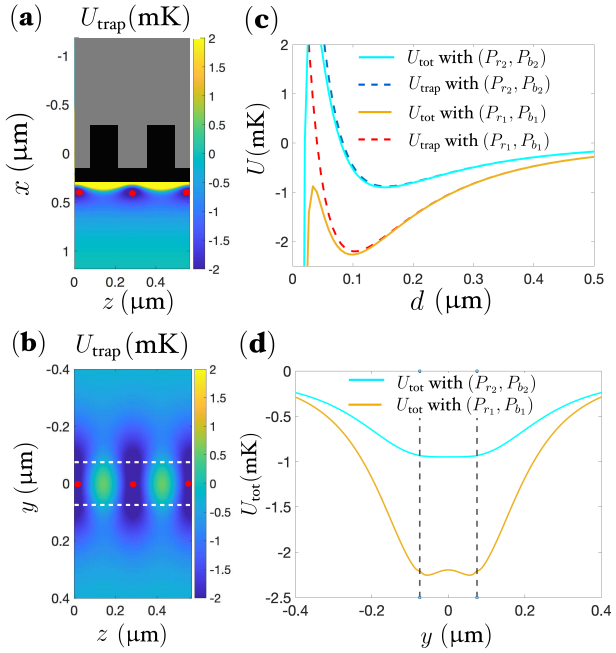

Fig. 5. Potential of the two-color trap. (a)-(b) Distribution of the trapping potential U_{trap} created by the superposition of the blue- and red-detuned modes. As in Fig. 4, we represent a cross-section in the (x, z) plane at $y = 0$ (a) and a cross-section in a (y, z) plane located in air at a distance $d = 100$ nm from the waveguide (b). Red dots represent atoms trapped in the potential wells. The black area in (a) shows the comb waveguide where the potential is not defined. We do not show the potential around the teeth (gray area); it is repulsive and does not exhibit trapping sites. The dashed lines in (b) remind the position of the GaInP membrane that is located in a different plane, shifted by 100 nm in the x direction. (c) Trapping potential U_{trap} (dashed curves) and total potential $U_{\text{tot}} = U_{\text{trap}} + U_{\text{CP}}$ (solid curves) as a function of the distance d to the waveguide for $y = 0$ and $z = 0 \pmod{a}$. Two different sets of trapping powers are represented. The powers $(P_{r_1}, P_{b_1}) = (1.6, 1.3)$ mW create a potential well at $d = 100$ nm with a depth $U \approx -2.2$ mK. The powers $(P_{r_2}, P_{b_2}) = (1, 1.3)$ mW create a potential well at $d = 160$ nm with a depth $U \approx -0.8$ mK. (d) Total potential U_{tot} as a function of the vertical coordinate y for $z = 0 \pmod{a}$. The orange (resp. light blue) curve shows the potential created at a distance $d = 100$ nm (resp. $d = 160$ nm) by blue- and red-detuned modes with powers (P_{r_1}, P_{b_1}) [resp. (P_{r_2}, P_{b_2})].

We have computed the trapping potential $U_{\text{trap}}(x, y, z)$ for Rb atoms with the recently-introduced open-source package Nanotrappy [65]. The inputs of Nanotrappy are the electric fields of the

blue- and red-detuned guided modes, which are calculated with the mode solver for periodic waveguides used to calculate the band diagram [49]. Nanotrappy calculates the Stark shifts induced by these electric fields and the corresponding potentials. The calculation includes the scalar, vector, and tensor shifts [65].

Figures 5(a)-(b) display maps of the trapping potential U_{trap} in the (x, z) plane at $y = 0$ and in a (y, z) plane located in air at a distance $d = 100$ nm from the structure. The powers of the red- and blue-detuned modes are respectively $(P_{r_1}, P_{b_1}) = (1.6, 1.3)$ mW. The potential is given in mK so that it can be easily compared with the temperature T of cold Rb atoms in a typical experiment, $T \sim 10$ μK. Red dots highlight the potential minima, where atoms can be trapped, at $y = 0$, $z = 0$ (mod $a = 283$ nm), and a distance $d = 100$ nm from the structure. The confinement is good in all three directions of space.

Finally, we investigate in Figs. 5(c)-(d) the impact on the trap of the powers of the detuned modes, as well as the effect of taking into account the CP potential. Cross-sections of U_{trap} (dashed curves) and $U_{\text{tot}} = U_{\text{trap}} + U_{\text{CP}}$ (solid curves) are plotted for two different sets of trapping powers $(P_{r_1}, P_{b_1}) = (1.6, 1.3)$ mW and $(P_{r_2}, P_{b_2}) = (1, 1.3)$ mW. Note that the power of the blue-detuned mode (i.e., the repulsive potential U_b) is kept constant. Decreasing the power of the red-detuned mode has two main effects. First, the depth of the potential well is reduced from ≈ 2.2 mK to ≈ 0.8 mK. Second, the trapping distance is increased from 100 nm to 160 nm. Adding the CP potential does not alter the potential well. It is only modified at shorter distances where the attracting CP interactions become dominant. For the closest trap ($d = 100$ nm, orange solid curve), the potential barrier between the trap and the structure is lowered by the CP interactions but it remains higher than 1 mK. The orange curve in Fig. 5(d) shows that the potential minimum is not necessarily located at $y = 0$. The height of the tiny potential barrier at $y = 0$ is only 50 μK

We have demonstrated the possibility to trap cold Rb atoms at deeply subwavelength distances ($d = 100$ nm) from the comb waveguide where the x-component of the electric field of the slow mode is intense. We have used a two-color optical trap with powers of about 1 mW, a value well compatible with the powers used in current integrated-optics experiments. We show in the following Section that an atom trapped at this position interacts strongly with the slow mode.

5. Strong atom-photon interaction

Having established the possibility to trap Rb atoms close to the comb waveguide, we now show that trapped atoms can strongly interact with the slow mode. For that purpose, we compute the spontaneous emission rate of an excited atom and the β factor – i.e., the fraction of light coupled to the slow mode.

With the optical trap discussed in Section 4, atoms are located at positions where the x-component of the electric field of the slow mode is dominant. Therefore, we consider in the following spontaneous emission of an atom with a dipole $\mathbf{d}$ that is linearly polarized along the x direction, $\mathbf{d} = d\mathbf{e}_x$ with $\mathbf{e}_x$ the unitary vector along the x direction. Experimentally, this situation can be realized by imposing a quantization axis along x with an external magnetic field.

We calculate the total emission rate Γ_{tot} and the emission rate in the slow mode Γ_{1D} (sum of the forward and backward propagation directions). The former is proportional to the imaginary part of the total Green tensor at the position $\mathbf{r}_0$ of the atom [66],

$$\frac{\Gamma_{\text{tot}}}{\Gamma_0} = \frac{6\pi c}{\omega_0} \mathbf{e}_x \cdot \text{Im}\left[\mathbf{G}(\mathbf{r}_0, \mathbf{r}_0, \omega_0)\right] \mathbf{e}_x, \tag{2}$$

while the latter depends only on the electric field of the guided mode [11, 35],

$$\frac{\Gamma_{\text{1D}}}{\Gamma_0} = \frac{n_g \sigma a \varepsilon_0 |\mathbf{e}_x \cdot \mathbf{E}_m^*(\mathbf{r}_0)|^2}{2 \iiint_{\text{Cell}} \varepsilon |\mathbf{E}_m|^2 d^3\mathbf{r}}. \tag{3}$$

In these expressions, ω_0 is the transition frequency, $\Gamma_0 = \omega_0^3|\mathbf{d}|^2/(3\pi\hbar\varepsilon_0 c^3)$ is the emission rate in vacuum, $\sigma = 3\lambda_0^2/(2\pi)$ is the absorption cross-section, $\mathbf{E}_m$ is the electric field of the slow mode, and $n_g = c/v_g$ is its group index. One usually defines the mode effective area as $A_{\text{eff}}(\mathbf{r}_0) = \iiint_{\text{Cell}} \varepsilon|\mathbf{E}_m|^2 d^3\mathbf{r}/(a\varepsilon_0|\mathbf{e}_x \cdot \mathbf{E}_m^*(\mathbf{r}_0)|^2)$. Note that the volume integral runs over one unit cell of the periodic waveguide.

Then, we deduce the emission rate outside the slow mode (i.e., into all the other modes), $\Gamma' = \Gamma_{\text{tot}} - \Gamma_{1\text{D}}$, as well as the value of the β factor, $\beta = \Gamma_{1\text{D}}/\Gamma_{\text{tot}}$. Let us recall that the slow mode supported by the comb waveguide designed in Section 3 has a group index $n_g = 50$ at the transition wavelength of Rb atoms, $\lambda_0 = 2\pi c/\omega_0 = 780$ nm. Its electric field is represented in Figs. 3(b)-(c).

The main difficulty is the calculation of the total Green tensor $\mathbf{G}(\mathbf{r}_0, \mathbf{r}_0, \omega_0)$ of an infinitely long periodic waveguide, which requires an accurate calculation of the emission into radiation modes with outgoing-wave conditions in a periodic medium [49]. Two different approaches are often used to bypass this difficulty. The first one amounts to assume that the emission rate into radiation modes is approximately equal to the emission rate in vacuum, $\Gamma' \approx \Gamma_0$, see for instance [13]. With this approximation, Eq. (2) simply becomes $\Gamma_{\text{tot}}/\Gamma_0 \approx 1 + \Gamma_{1\text{D}}/\Gamma_0$. In that case, the calculation only requires the knowledge of the guided mode, which can be calculated with a Bloch-mode solver. The second approach that avoids the calculation of the Green tensor of an infinitely long periodic waveguide consists in considering a finite-size structure formed by a finite number of periods, see for instance [37]. The main drawback is that the calculated structure (a Fabry-Perot cavity) is different from the desired one (an infinitely long waveguide). As a result, the emission rate exhibits a series of spurious resonance peaks that depends on the arbitrary choice of the structure length and termination. It is thus difficult to infer the actual emission rate of the periodic waveguide.

In contrast to these two approximate approaches, we calculate rigorously the Green tensor of the periodic waveguide by using a modal method that relies on an exact Bloch-mode expansion [49]. Figure 6 shows the variation of the decay rates Γ_{tot}, $\Gamma_{1\text{D}}$, Γ' (first line), and of the β factor (second line) as a function of the position of the atom. In Fig. 6(a), the atom is moved horizontally away from the comb for $y = 0$ and $z = 0$ (mod a). In Fig. 6(b), the atom is moved vertically for $d = 100$ nm and $z = 0$ (mod a). In Fig. 6(c), the atom is moved along the waveguide for $d = 100$ nm and $y = 0$. The yellow areas represent the volume where atoms are likely to be trapped, defined as the positions where the value of the orange potential in Fig. 5 is between $U_{min} \approx -2.2$ mK and $U_{min} + 50$ μK. This defines a trapping volume of typical size 30 nm along x, 160 nm along y and 20 nm along z.

For large distances, $d > 400$ nm, the emission rate $\Gamma_{1\text{D}}$ into the slow mode is negligible compared to the emission rate Γ' into the radiation continuum and the β factor tends towards zero. As the distance d decreases, the atom enters the region where the field of the slow mode is intense and Figs. 6(a) shows a strong enhancement of $\Gamma_{1\text{D}}$ that results in an increase of the β factor. For a trapping distance of $d = 100$ nm (yellow area), $\Gamma_{1\text{D}} = 10\Gamma_0$, $\Gamma' = 1.3\Gamma_0$, and $\beta = 0.88$. This number is significantly larger than the value of $\beta \approx 0.5$ that has been experimentally observed for the alligator waveguide [12, 60].

In Figs. 6(b)-(c), we fix the distance $d = 100$ nm and we vary the position of the atom in the two other directions. Along the vertical direction, as long as the atom is located inside the trap in front of the structure (-75 nm $\leqslant y \leqslant 75$ nm), the decay rate into the slow mode remains dominant $\Gamma_{1\text{D}} > 8\Gamma_0$ and $\beta > 0.8$. Along the z direction, $\Gamma_{1\text{D}}$ varies periodically. Its variation over one period is directly related to the variation of $|E_x(z)|$ represented in Fig. 3(b). On the other hand, Γ' is almost constant.

Finally, let us emphasize that the presence of the comb increases the emission rate into the radiation continuum Γ', compared to the emission rate in vacuum Γ_0. Indeed, for $d \leqslant 100$ nm and -75 nm $\leqslant y \leqslant 75$ nm, $\Gamma' \geqslant 1.3\Gamma_0$. Therefore, the assumption $\Gamma' \approx \Gamma_0$ would lead to an error

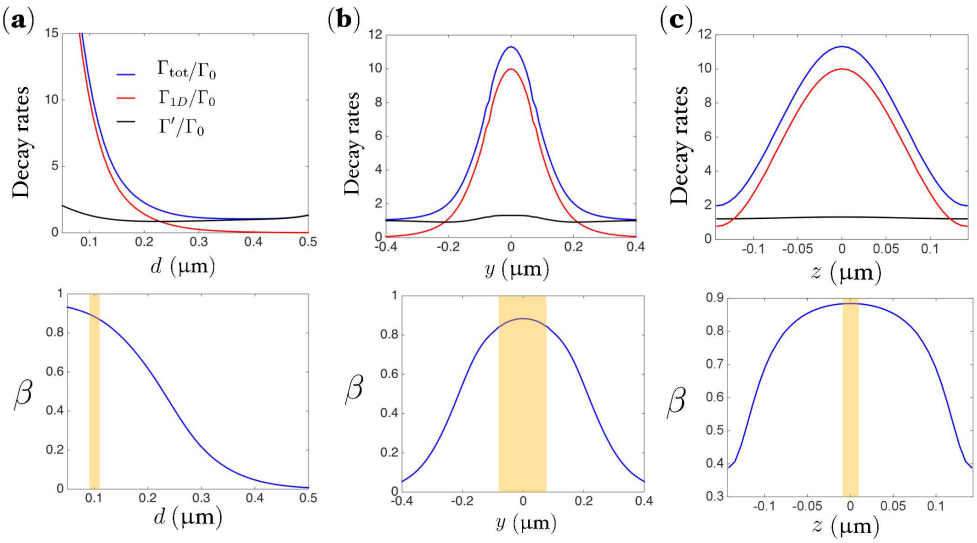

Fig. 6. Decay rates of an atom near the 3D asymmetric comb waveguide. First line: Decay rates Γ_{tot} (blue), $\Gamma_{1\text{D}}$ (red), and Γ' (black) as a function of the distance d from the waveguide for $y = 0$ and $z = 0$ (mod a) (a), as a function of y for $d = 100$ nm and $z = 0$ (mod a) (b), and as a function of z for $d = 100$ nm and $y = 0$ (c). All decay rates are normalized by the decay rate Γ_0 of the atom in vacuum. Second line: Variation of the β factor, $\beta = \Gamma_{1\text{D}}/\Gamma_{\text{tot}}$, at the same positions. The yellow areas represent the volume where atoms are likely to be trapped, defined as the positions where the value of the orange potential in Fig. 5 is between $U_{min} \approx -2.2$ mK and $U_{min} + 50$ μK.

larger than 30% for $d \leqslant 100$ nm. This trend of an increase of Γ' close to a dielectric structure is not general; a previous calculation with the same numerical method has shown a decrease of Γ' in the near field of a different periodic waveguide [67].

6. Conclusion

We have proposed a new waveguide geometry, the asymmetric comb, that provides a strong interaction between trapped atoms and guided photons. An important originality of the structure is its quartic dispersion relation of the form $\omega - \omega_e \propto -(k - \pi/a)^4$, unique in the context of waveguide QED. We have demonstrated that this specific form of the dispersion relation reduces the impact of the inevitable fabrication imperfections. Then, we have shown how cold Rubidium atoms can be trapped at subwavelength distances ($d = 100$ nm) from the structure by implementing a two-color optical trap with guided modes that are red and blue detuned with respect to the atomic transition frequency. Finally, we have completely characterized the decay of an excited atom in this complex photonic environment by calculating rigorously the decay rate $\Gamma_{1\text{D}}$ into the guided mode as well as the decay rate Γ' into all other radiative channels. Atoms inside the trap decay preferentially into the slow mode (group velocity $v_g = c/50$) with a β factor as high as 0.88.

We have considered throughout the article a structure made of GaInP, a semiconductor material with a high refractive index. This choice is not critical for the design. We have checked that an asymmetric comb waveguide with a quartic dispersion and a large β factor can also be designed in a material with a lower refractive index such as silicon nitride or silicon oxide. Regarding the fabrication, we have conducted preliminary studies (not shown here) that show that the fabrication of the structure is completely feasible with current fabrication processes. Note that

suspended periodic waveguides with symmetrical patterns of similar dimensions have been fabricated in [47]. Two important practical issues are the coupling of light into the slow mode and its propagation loss. Attenuations of 3 dB after propagation over 100 μm have been measured for $n_g = 50$ in a photonic-crystal waveguide [57]. We can reasonably expect lower propagation loss since we have shown that the asymmetric comb waveguide has a larger effective photon mass. Coupling light into the slow mode can be achieved by gradually decreasing the group velocity with an adiabatic tuning of the waveguide geometry. Short (1–2 μm) and efficient (90% efficiency) tapers have been realized with this strategy [68–70].

Being able to control the emission with figures of merit as large as $\Gamma_{1D} = 10\Gamma_0$, $\Gamma' = 1.3\Gamma_0$, and $\beta = 0.88$ puts the strong coupling regime of waveguide QED ($\Gamma_{1D}/\Gamma' \gg 1$) within reach. In this important regime, both collective [71–76] and non-linear quantum [2] phenomena are enhanced, meaning that single photon switches [77] or coherent photon storage [17,18,29] could be achieved with high efficiencies. Exotic many-body phenomena such as correlated photon transport [21], many-body localization [26], or fermionization of the multiple excited states [78] could also be explored with the asymmetric comb. Finally, let us emphasize that the uncommon dispersion relation of the slow mode significantly alters the range of the photon-mediated interactions for atoms whose transition frequencies lie inside the bandgap, as discussed in Supplement 1. Enlarging the bandwidth of the structure also allows one to probe with reduced distortion the fast dynamics of superradiant emission.

Funding. This work was supported by the French National Research Agency (ANR) under the NanoStrong Project (ANR-18-CE47-0008) and the Région Ile-de-France (DIM SIRTEQ). This project has also received funding from the European Union Horizon 2020 research and innovation programme under Grant Agreement No. 899275 (DAALI project). A.U. was supported by the European Union (Marie Curie Fellowship SinglePass 101030421).

Disclosures. The authors declare no conflicts of interest.

Data availability. Data underlying the results presented in this paper are not publicly available at this time but may be obtained from the authors upon reasonable request.

Supplemental document. See Supplement 1 for supporting content.

References

1. H. J. Kimble, "The quantum internet," Nature **453**, 1023–1030 (2008).
2. D. E. Chang, V. Vuletić, and M. D. Lukin, "Quantum nonlinear optics—photon by photon," Nat. Photonics **8**, 685–694 (2014).
3. J.-M. Raimond, M. Brune, and S. Haroche, "Manipulating quantum entanglement with atoms and photons in a cavity," Rev. Mod. Phys. **73**, 565–582 (2001).
4. A. Reiserer and G. Rempe, "Cavity-based quantum networks with single atoms and optical photons," Rev. Mod. Phys. **87**, 1379–1418 (2015).
5. J.-M. Gérard, B. Sermage, B. Gayral, B. Legrand, E. Costard, and V. Thierry-Mieg, "Enhanced spontaneous emission by quantum boxes in a monolithic optical microcavity," Phys. Rev. Lett. **81**, 1110–1113 (1998).
6. P. Lodahl, S. Mahmoodian, and S. Stobbe, "Interfacing single photons and single quantum dots with photonic nanostructures," Rev. Mod. Phys. **87**, 347–400 (2015).
7. T. G. Tiecke, J. D. Thompson, N. P. de Leon, L. R. Liu, V. Vuletić, and M. D. Lukin, "Nanophotonic quantum phase switch with a single atom," Nature **508**, 241–244 (2014).
8. K. P. Nayak, P. N. Melentiev, M. Morinaga, F. Le Kien, V. I. Balykin, and K. Hakuta, "Optical nanofiber as an efficient tool for manipulating and probing atomic fluorescence," Opt. Express **15**, 5431–5438 (2007).
9. E. Vetsch, D. Reitz, G. Sagué, R. Schmidt, S. T. Dawkins, and A. Rauschenbeutel, "Optical interface created by laser-cooled atoms trapped in the evanescent field surrounding an optical nanofiber," Phys. Rev. Lett. **104**, 203603 (2010).
10. A. Goban, K. S. Choi, D. J. Alton, D. Ding, C. Lacroûte, M. Pototschnig, T. Thiele, N. P. Stern, and H. J. Kimble, "Demonstration of a state-insensitive, compensated nanofiber trap," Phys. Rev. Lett. **109**, 033603 (2012).
11. A. Goban, C.-L. Hung, S.-P. Yu, J. D. Hood, J. A. Muniz, J. H. Lee, M. J. Martin, A. C. McClung, K. S. Choi, D. E. Chang, O. Painter, and H. J. Kimble, "Atom–light interactions in photonic crystals," Nat. Commun. **5**, 3808 (2014).
12. A. Goban, C.-L. Hung, J. D. Hood, S.-P. Yu, J. A. Muniz, O. Painter, and H. J. Kimble, "Superradiance for atoms trapped along a photonic crystal waveguide," Phys. Rev. Lett. **115**, 063601 (2015).

13. X. Zang, J. Yang, R. Faggiani, C. Gill, P. G. Petrov, J.-P. Hugonin, K. Vynck, S. Bernon, P. Bouyer, V. Boyer, and P. Lalanne, "Interaction between atoms and slow light: a study in waveguide design," Phys. Rev. Appl. **5**, 024003 (2016).
14. D. Roy, C. M. Wilson, and O. Firstenberg, "Colloquium: Strongly interacting photons in one-dimensional continuum," Rev. Mod. Phys. **89**, 021001 (2017).
15. D. E. Chang, J. S. Douglas, A. González-Tudela, C.-L. Hung, and H. J. Kimble, "Colloquium: Quantum matter built from nanoscopic lattices of atoms and photons," Rev. Mod. Phys. **90**, 031002 (2018).
16. P. Türschmann, H. Le Jeannic, S. F. Simonsen, H. R. Haakh, S. Götzinger, V. Sandoghdar, P. Lodahl, and N. Rotenberg, "Coherent nonlinear optics of quantum emitters in nanophotonic waveguides," Nanophotonics **8**, 1641–1657 (2019).
17. B. Gouraud, D. Maxein, A. Nicolas, O. Morin, and J. Laurat, "Demonstration of a memory for tightly guided light in an optical nanofiber," Phys. Rev. Lett. **114**, 180503 (2015).
18. C. Sayrin, C. Clausen, B. Albrecht, P. Schneeweiss, and A. Rauschenbeutel, "Storage of fiber-guided light in a nanofiber-trapped ensemble of cold atoms," Optica **2**, 353–356 (2015).
19. N. V. Corzo, J. Raskop, A. Chandra, A. S. Sheremet, B. Gouraud, and J. Laurat, "Waveguide-coupled single collective excitation of atomic arrays," Nature **566**, 359–362 (2019).
20. S. Mahmoodian, M. Čepulkovskis, S. Das, P. Lodahl, K. Hammerer, and A. S. Sørensen, "Strongly correlated photon transport in waveguide quantum electrodynamics with weakly coupled emitters," Phys. Rev. Lett. **121**, 143601 (2018).
21. S. Mahmoodian, G. Calajó, D. E. Chang, K. Hammerer, and A. S. Sørensen, "Dynamics of many-body photon bound states in chiral waveguide qed," Phys. Rev. X **10**, 031011 (2020).
22. A. S. Prasad, J. Hinney, S. Mahmoodian, K. Hammerer, S. Rind, P. Schneeweiss, A. S. Sørensen, J. Volz, and A. Rauschenbeutel, "Correlating photons using the collective nonlinear response of atoms weakly coupled to an optical mode," Nat. Photonics **14**, 719–722 (2020).
23. J. S. Douglas, H. Habibian, C.-L. Hung, A. V. Gorshkov, H. J. Kimble, and D. E. Chang, "Quantum many-body models with cold atoms coupled to photonic crystals," Nat. Photonics **9**, 326–331 (2015).
24. G. Calajó and D. E. Chang, "Emergence of solitons from many-body photon bound states in quantum nonlinear media," Phys. Rev. Res. **4**, 023026 (2022).
25. B. Bakkensen, Y.-X. Zhang, J. Bjerlin, and A. S. Sørensen, "Photonic bound states and scattering resonances in waveguide QED," arXiv preprint arXiv:2110.06093 (2021).
26. N. Fayard, L. Henriet, A. Asenjo-Garcia, and D. E. Chang, "Many-body localization in waveguide quantum electrodynamics," Phys. Rev. Res. **3**, 033233 (2021).
27. H. L. Sørensen, J.-B. Béguin, K. W. Kluge, I. Iakoupov, A. S. Sørensen, J. H. Müller, E. S. Polzik, and J. Appel, "Coherent backscattering of light off one-dimensional atomic strings," Phys. Rev. Lett. **117**, 133604 (2016).
28. N. V. Corzo, B. Gouraud, A. Chandra, A. Goban, A. S. Sheremet, D. V. Kupriyanov, and J. Laurat, "Large bragg reflection from one-dimensional chains of trapped atoms near a nanoscale waveguide," Phys. Rev. Lett. **117**, 133603 (2016).
29. P. Solano, P. Barberis-Blostein, F. K. Fatemi, L. A. Orozco, and S. L. Rolston, "Super-radiance reveals infinite-range dipole interactions through a nanofiber," Nat. Commun. **8**, 1857 (2017).
30. V. I. Balykin, K. Hakuta, F. Le Kien, J. Q. Liang, and M. Morinaga, "Atom trapping and guiding with a subwavelength-diameter optical fiber," Phys. Rev. A **70**, 011401 (2004).
31. F. Le Kien, V. I. Balykin, and K. Hakuta, "Atom trap and waveguide using a two-color evanescent light field around a subwavelength-diameter optical fiber," Phys. Rev. A **70**, 063403 (2004).
32. T. Nieddu, V. Gokhroo, and S. N. Chormaic, "Optical nanofibres and neutral atoms," J. Opt. **18**, 053001 (2016).
33. P. Forn-Díaz, L. Lamata, E. Rico, J. Kono, and E. Solano, "Ultrastrong coupling regimes of light-matter interaction," Rev. Mod. Phys. **91**, 025005 (2019).
34. A. S. Sheremet, M. I. Petrov, I. V. Iorsh, A. V. Poshakinskiy, and A. N. Poddubny, "Waveguide quantum electrodynamics: collective radiance and photon-photon correlations," arXiv preprint arXiv:2103.06824 (2021).
35. G. Lecamp, P. Lalanne, and J.-P. Hugonin, "Very large spontaneous-emission β factors in photonic-crystal waveguides," Phys. Rev. Lett. **99**, 023902 (2007).
36. J. D. Joannopoulos, S. G. Johnson, J. N. Winn, and R. D. Meade, *Molding the flow of light* (Princeton University, 2008), chap. 7.
37. C.-L. Hung, S. M. Meenehan, D. E. Chang, O. Painter, and H. J. Kimble, "Trapped atoms in one-dimensional photonic crystals," New J. Phys. **15**, 083026 (2013).
38. S.-P. Yu, J. D. Hood, J. A. Muniz, M. J. Martin, R. Norte, C.-L. Hung, S. M. Meenehan, J. D. Cohen, O. Painter, and H. J. Kimble, "Nanowire photonic crystal waveguides for single-atom trapping and strong light-matter interactions," Appl. Phys. Lett. **104**, 111103 (2014).
39. J.-B. Beguin, A. P. Burgers, X. Luan, Z. Qin, S. P. Yu, and H. J. Kimble, "Advanced apparatus for the integration of nanophotonics and cold atoms," Optica **7**, 1–2 (2020).
40. R. Faggiani, A. Baron, X. Zang, L. Lalouat, S. A. Schulz, B. O'Regan, K. Vynck, B. Cluzel, F. de Fornel, T. F. Krauss, and P. Lalanne, "Lower bound for the spatial extent of localized modes in photonic crystal waveguides with small random imperfections," Sci. Reports **6**, 27037 (2016).
41. M. Loncar, D. Nedeljkovic, T. Doll, J. Vuckovic, A. Scherer, and T. Pearsall, "Waveguiding in planar photonic crystals," Appl. Phys. Lett. **77**, 1937–1939 (2000).
42. M. Notomi, K. Yamada, A. Shinya, J. Takahashi, C. Takahashi, and I. Yokohama, "Extremely large group-velocity

dispersion of line-defect waveguides in photonic crystal slabs," Phys. Rev. Lett. **87**, 253902 (2001).
43. M. Gnan, W. C. L. Hopman, G. Bellanca, R. M. de Ridder, R. M. De La Rue, and P. Bassi, "Closure of the stop-band in photonic wire bragg gratings," Opt. Express **17**, 8830–8842 (2009).
44. P. J. Bock, P. Cheben, J. H. Schmid, J. Lapointe, A. Delage, S. Janz, G. C. Aers, D.-X. Xu, A. Densmore, and T. J. Hall, "Subwavelength grating periodic structures in silicon-on-insulator: a new type of microphotonic waveguide," Opt. Express **18**, 20251–20262 (2010).
45. M. Ibrahim, J. H. Schmid, A. Aleali, P. Cheben, J. Lapointe, S. Janz, P. J. Bock, A. Densmore, A. Lamontagne, R. Ma, D.-X. Xu, and W. N. Ye, "Athermal silicon waveguides with bridged subwavelength gratings for TE and TM polarizations," Opt. Express **20**, 18356–18361 (2012).
46. J. S. Penadés, C. Alonso-Ramos, A. Z. Khokhar, M. Nedeljkovic, L. A. Boodhoo, A. Ortega-Moñux, I. Molina-Fernández, P. Cheben, and G. Z. Mashanovich, "Suspended soi waveguide with sub-wavelength grating cladding for mid-infrared," Opt. Lett. **39**, 5661–5664 (2014).
47. C. Alonso-Ramos, X. Le Roux, J. Zhang, D. Benedikovic, V. Vakarin, E. Durán-Valdeiglesias, D. Oser, D. Pérez-Galacho, F. Mazeas, L. Labonté, S. Tanzilli, E. Cassan, D. Marris-Morini, P. Cheben, and L. Vivien, "Diffraction-less propagation beyond the sub-wavelength regime: a new type of nanophotonic waveguide," Sci. Reports **9**, 5347 (2019).
48. H. S. Nguyen, F. Dubois, T. Deschamps, S. Cueff, A. Pardon, J.-L. Leclercq, C. Seassal, X. Letartre, and P. Viktorovitch, "Symmetry breaking in photonic crystals: On-demand dispersion from flatband to dirac cones," Phys. Rev. Lett. **120**, 066102 (2018).
49. G. Lecamp, J.-P. Hugonin, and P. Lalanne, "Theoretical and computational concepts for periodic optical waveguides," Opt. Express **15**, 11042–11060 (2007).
50. E. Silberstein, P. Lalanne, J.-P. Hugonin, and Q. Cao, "Use of grating theories in integrated optics," J. Opt. Soc. Am. A **18**, 2865–2875 (2001).
51. J.-P. Hugonin and P. Lalanne, "Perfectly matched layers as nonlinear coordinate transforms: a generalized formalization," J. Opt. Soc. Am. A **22**, 1844–1849 (2005).
52. S. Hughes, L. Ramunno, J. F. Young, and J. E. Sipe, "Extrinsic optical scattering loss in photonic crystal waveguides: Role of fabrication disorder and photon group velocity," Phys. Rev. Lett. **94**, 033903 (2005).
53. J. Topolancik, B. Ilic, and F. Vollmer, "Experimental observation of strong photon localization in disordered photonic crystal waveguides," Phys. Rev. Lett. **99**, 253901 (2007).
54. S. Mazoyer, J.-P. Hugonin, and P. Lalanne, "Disorder-induced multiple scattering in photonic-crystal waveguides," Phys. Rev. Lett. **103**, 063903 (2009).
55. M. Patterson, S. Hughes, S. Combrié, N.-V.-Q. Tran, A. De Rossi, R. Gabet, and Y. Jaouën, "Disorder-induced coherent scattering in slow-light photonic crystal waveguides," Phys. Rev. Lett. **102**, 253903 (2009).
56. P. D. García, S. Smolka, S. Stobbe, and P. Lodahl, "Density of states controls Anderson localization in disordered photonic crystal waveguides," Phys. Rev. B **82**, 165103 (2010).
57. S. Mazoyer, P. Lalanne, J.-C. Rodier, J.-P. Hugonin, M. Spasenović, L. Kuipers, D. M. Beggs, and T. F. Krauss, "Statistical fluctuations of transmission in slow light photonic-crystal waveguides," Opt. Express **18**, 14654–14663 (2010).
58. A. P. Burgers, L. S. Peng, J. A. Muniz, A. C. McClung, M. J. Martin, and H. J. Kimble, "Clocked atom delivery to a photonic crystal waveguide," Proc. National Acad. Sci. **116**, 456–465 (2019).
59. J.-B. Beguin, J. Laurat, X. Luan, A. P. Burgers, Z. Qin, and H. J. Kimble, "Reduced volume and reflection for bright optical tweezers with radial Laguerre–Gauss beams," Proc. National Acad. Sci. **117**, 26109–26117 (2020).
60. J. D. Hood, A. Goban, A. Asenjo-Garcia, M. Lu, S.-P. Yu, D. E. Chang, and H. J. Kimble, "Atom–atom interactions around the band edge of a photonic crystal waveguide," Proc. National Acad. Sci. **113**, 10507–10512 (2016).
61. H. B. G. Casimir and D. Polder, "The influence of retardation on the London-van der Waals forces," Phys. Rev. **73**, 360–372 (1948).
62. S. Y. Buhmann and D.-G. Welsch, "Dispersion forces in macroscopic quantum electrodynamics," Prog. Quantum Electron. **31**, 51–130 (2007).
63. A. O. Caride, G. L. Klimchitskaya, V. M. Mostepanenko, and S. I. Zanette, "Dependences of the van der Waals atom-wall interaction on atomic and material properties," Phys. Rev. A **71**, 042901 (2005).
64. M. Schubert, V. Gottschalch, C. M. Herzinger, H. Yao, P. G. Snyder, and J. A. Woollam, "Optical constants of $Ga_xIn_{1-x}P$ lattice matched to GaAs," J. Appl. Phys. **77**, 3416–3419 (1995).
65. J. Berroir, A. Bouscal, A. Urvoy, T. Ray, and J. Laurat, "Nanotrappy: An open-source versatile package for cold-atom trapping close to nanostructures," Phys. Rev. Res. **4**, 013079 (2022).
66. L. Novotny and B. Hecht, *Principles of Nano-Optics* (Cambridge University, 2006), 2nd ed.
67. X. Zang and P. Lalanne, "Theoretical treatment of the interaction between two-level atoms and periodic waveguides," Opt. Lett. **40**, 3869–3872 (2015).
68. J.-P. Hugonin, P. Lalanne, T. P. White, and T. F. Krauss, "Coupling into slow-mode photonic crystal waveguides," Opt. Lett. **32**, 2638–2640 (2007).
69. P. Pottier, M. Gnan, and R. M. De La Rue, "Efficient coupling into slow-light photonic crystal channel guides using photonic crystal tapers," Opt. Express **15**, 6569–6575 (2007).
70. C. M. de Sterke, J. Walker, K. B. Dossou, and L. C. Botten, "Efficient slow light coupling into photonic crystals," Opt. Express **15**, 10984–10990 (2007).

71. D. Plankensteiner, L. Ostermann, H. Ritsch, and C. Genes, "Selective protected state preparation of coupled dissipative quantum emitters," Sci. Reports **5**, 16231 (2015).
72. A. Asenjo-Garcia, M. Moreno-Cardoner, A. Albrecht, H. J. Kimble, and D. E. Chang, "Exponential improvement in photon storage fidelities using subradiance and "selective radiance" in atomic arrays," Phys. Rev. X **7**, 031024 (2017).
73. D. F. Kornovan, N. V. Corzo, J. Laurat, and A. S. Sheremet, "Extremely subradiant states in a periodic one-dimensional atomic array," Phys. Rev. A **100**, 063832 (2019).
74. I. Shlesinger, P. Senellart, L. Lanco, and J.-J. Greffet, "Time-frequency encoded single-photon generation and broadband single-photon storage with a tunable subradiant state," Optica **8**, 95–105 (2021).
75. G. Ferioli, A. Glicenstein, L. Henriet, I. Ferrier-Barbut, and A. Browaeys, "Storage and release of subradiant excitations in a dense atomic cloud," Phys. Rev. X **11**, 021031 (2021).
76. M. Reitz, C. Sommer, and C. Genes, "Cooperative quantum phenomena in light-matter platforms," PRX Quantum **3**, 010201 (2022).
77. D. E. Chang, A. S. Sørensen, E. A. Demler, and M. D. Lukin, "A single-photon transistor using nanoscale surface plasmons," Nat. Phys. **3**, 807–812 (2007).
78. A. Albrecht, L. Henriet, A. Asenjo-Garcia, P. B. Dieterle, O. Painter, and D. E. Chang, "Subradiant states of quantum bits coupled to a one-dimensional waveguide," New J. Phys. **21**, 025003 (2019).